

Span Efficiencies of Wings at Low Reynolds Numbers

G. R. Spedding* and J. McArthur†

University of Southern California, Los Angeles, Los Angeles California 90089-1191

DOI: 10.2514/1.44247

Elegant and inviscid analytical theory can predict the induced drag on lifting wings of finite span. The theoretical prediction is then often modified by multiplication with a dimensionless coefficient for which the departure from a value of 1 is used as a way to incorporate realistic and necessary departures from the idealized model. Unfortunately, there are conflicting definitions of these dimensionless coefficients, often known as span efficiencies, so that even if numerical values are assigned in a clear and transparent fashion, their application and validity remain unclear. Here, the differences between two commonly used definitions of span efficiency are identified and it is shown that for the case of airfoil sections and finite wings at chordwise Reynolds numbers less than 10^5 , neither one has values close to those commonly assumed in the aeronautics literature. The cause of these significant viscous modifications to inviscid theory is traced to the movement of separation points from the trailing edge of real airfoils. A modified nomenclature is suggested to reduce the likelihood of confusion, and appropriate formulations for the drag of streamlined bodies in viscous flows at moderate Reynolds number are considered, with application to small-scale flying devices, both natural and engineered.

Nomenclature

A	= drag-polar fitting coefficient
AR	= aspect ratio
a_0	= offset in general quadratic curve fit
a_2	= coefficient for quadratic polar fit
B	= drag-polar fitting coefficient
b	= wingspan
C_D	= total drag coefficient on a finite wing
$C_{D,i}$	= induced drag coefficient on a finite wing
$C_{D,0}$	= minimum total drag coefficient on a finite wing
C_d	= section drag coefficient
$C_{d,0}$	= minimum section drag coefficient
C_L	= lift coefficient for finite wing
$C_{L\alpha}$	= lift slope for finite wing
C_l	= section lift coefficient
$C_{l\alpha}$	= sectional lift slope of $C_l(\alpha)$
$C_{l,0}$	= minimum section lift coefficient
c	= mean wing chord
D	= drag force (opposed to U)
D_i	= induced drag
e	= Oswald or span efficiency
e_i	= inviscid span efficiency
e_v	= viscous span efficiency
k	= fitting coefficient for section polar $C_d(C_l)$
k	= induced-power factor
k_i	= inviscid power factor ($1/e_i$)
k_v	= viscous power factor ($1/e_v$)
L	= total lift
q	= dynamic pressure
Re	= Reynolds number
S	= wing planform area
S_d	= actuator disk area
U	= mean flight speed
u'	= rms fluctuating velocity

W	= weight
α	= geometric angle of attack
α_i	= increase in angle of attack due to induced drag
α'	= angle of attack (difference from α at $L = 0$)
β	= power-law exponent
δ	= boundary-layer thickness
δ	= small parameter for inviscid wing efficiency
ν	= kinematic viscosity

I. Introduction

THE foundations of aeronautics are laid on steady flows around fixed bodies at moderately high values of Reynolds number ($Re = Uc/\nu$, where U is a mean flight speed, c is a mean flightwise chord length, and ν is the kinematic viscosity). Reynolds numbers for various aircraft components (wings, tail, and fuselage) are given in [1], for example, and on aerodynamic surfaces, range from approximately 2×10^6 (vertical tail of the Cessna Stationair 7 at sea level, flaps down) to 80×10^6 (wing of the Boeing 747-200B, at maximum cruise speed, 10 km height). At these Reynolds numbers, the boundary-layer thickness δ is on the order of 10 mm ($\delta/c \approx 3 \times 10^{-4}$), and at low angles of attack α , the elegant analyses of thin-airfoil theory apply very well, in which various geometric approximations and the prescription of zero normal velocity to the surface, together with the Kutta condition at the trailing edge, lead to closed-form solutions for circulation distributions on thin airfoils and simple numerical solutions for arbitrarily shaped bodies.

II. List and Drag of Finite Wings

A. Lifting Line and the Drag of Finite Aspect Ratio Wings

Of course, inviscid models also predict that the drag $D = 0$, at least in two-dimensional flows. Much effort has been put into the empirical compilation and verification of drag polars, plots of the sectional lift vs sectional drag coefficient for two-dimensional (2-D) airfoils, or section profiles. For wings of finite span, one can also show that there is an inviscid source of drag, the induced drag, which can be written in coefficient form,

$$C_{D,i} = \frac{C_L^2}{\pi AR} \quad (1)$$

for the special case of an elliptically loaded wing. The induced drag coefficient $C_{D,i} = D_i/qS$ is normalized by the planform area S and dynamic pressure $q = \rho U^2/2$, where ρ is the air density. Similarly, the lift coefficient $C_L = L/qS$, where L is the lift force normal to the direction of mean flight speed U . (Sectional, or 2-D, coefficients of

Received 9 March 2009; revision received 8 May 2009; accepted for publication 8 May 2009. Copyright © 2009 by the American Institute of Aeronautics and Astronautics, Inc. All rights reserved. Copies of this paper may be made for personal or internal use, on condition that the copier pay the \$10.00 per-copy fee to the Copyright Clearance Center, Inc., 222 Rosewood Drive, Danvers, MA 01923; include the code 0021-8669/10 and \$10.00 in correspondence with the CCC.

*Department of Aerospace and Mechanical Engineering; geoff@usc.edu. Member AIAA.

†Department of Aerospace and Mechanical Engineering; currently Advanced Systems Aeronautical Group, Aerovironment, Inc., Simi Valley, CA 91501; mcarthur@avinc.com.

lift and drag are denoted as C_l and C_d , respectively, and now L and D are normalized by qc , rather than qS , and so their coefficients have units of normalized force per unit span.) In Eq. (1), AR is the aspect ratio, defined either as $AR = b^2/S$ or b/c . The experimental verification of the variation of $C_{D,i}$ with $1/AR$ was provided by Prandtl [2]. For wings that are not elliptically loaded, Eq. (1) may be written [3]

$$C_{D,i} = \frac{C_L^2}{\pi AR} (1 + \delta) \quad (2)$$

where δ is a small number that measures the departure of the loading distribution from elliptic. It can be estimated numerically from a sum of the Fourier coefficients describing the wing circulation distribution. Equation (2) is often expressed as

$$C_{D,i} = \frac{C_L^2}{\pi AR e} \quad (3)$$

and $e = 1/(1 + \delta)$ is called the span efficiency factor. It measures the departure of the loading from its elliptic optimum for the inviscid induced drag of a finite wing, when $e = 1$. The condition for $e = 1$ is only that the circulation distribution along the span be elliptic, which, for a wing with constant profile shape, can come from planform geometry or from wing twist. The effects of aspect ratio are not included in e , which also does not have any contributions from other sources of drag than induced drag.

The remaining sources of drag, other than Eq. (3), are all due in some way to viscosity and cannot be predicted in inviscid models. Instead, drag polars are compiled for various two-dimensional profiles and for various wing shapes, and a sketch is shown in Fig. 1 for a two-dimensional section profile and for a wing of finite aspect ratio. For the 2-D airfoil, a $C_l(C_d)$ polar is derived by changing the geometric angle of attack α . For the general asymmetric case, the drag is a minimum at some (usually positive) α , when C_l will also have some finite value (as shown in Fig. 1). For α different from this value, then the variation of C_l with C_d can be described by

$$C_d = C_{d,0} + k(C_l - C_{l,0})^2 \quad (4)$$

where $C_{d,0}$ and $C_{l,0}$ are the drag and lift values at minimum drag (so $C_{d,0} = C_{d,\min}$). Then the total drag of a wing of finite span can be written

$$C_D = C_{D,0} + kC_L^2 + \frac{C_L^2}{\pi AR} (1 + \delta) \quad (5)$$

The third term on the right-hand side derives from Eq. (3); it is the induced drag multiplied by the correction for nonelliptic loading. The first term on the right-hand side is a minimum constant drag and its value is usually indistinguishable from the two-dimensional equivalent (see Fig. 1), and so we may set $C_{D,0} \approx C_{d,0}$. The second term has k from Eq. (4), which gives the quadratic rise in C_d with $C_l - C_{l,0}$. Two simplifying assumptions are made in Eq. (5): first, that $C_l \approx C_l - C_{l,0}$, and second, that the same k can be used for 2-D and 3-D wings. This is equivalent to requiring that the reduction in α due to induced drag is small, so that $\alpha \approx \alpha - \alpha_i$. Because C_L^2 appears in the last two terms in Eq. (5), one can also find this equation in the literature (e.g., [1,4]) expressed as

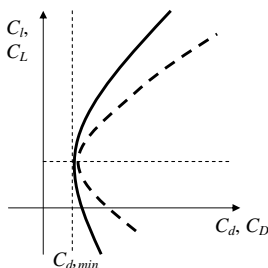


Fig. 1 Hypothetical drag polars for 2-D profile [$C_l(C_d)$, continuous line] and finite wing [$C_L(C_D)$, dashed line].

$$C_D = C_{D,0} + \frac{C_L^2}{\pi AR e} \quad (6)$$

where

$$e = 1/(1 + \delta + k\pi AR) \quad (7)$$

This e may be referred to as the Oswald efficiency factor, or sometimes as the span efficiency, even though it is not the same as e in Eq. (3), because it contains corrections not only from departures from elliptical loading δ , but also from finite AR and from the presumed parabolic shape of the section lift–drag polar k .

Alternatively, the total drag of a wing can also be written correctly (e.g., [5]) using Eq. (3) as

$$C_D = C_d + \frac{C_L^2}{\pi AR e} \quad (8)$$

which is quite different from Eq. (6). Here, e is only the correction for nonelliptic loading, as introduced in Eq. (3), and it does not contain any implicit information about the variation of C_d with C_l . Instead, the value of C_d is read from drag polars for the appropriate α , which should be corrected for α_i . Von Mises [6] introduced an apparently similar formulation as

$$C_D = A + \frac{C_L^2}{B} \quad (9)$$

noting that A depends mainly on the shape of the profile, and B depends mainly on aspect ratio. However, A is identified as a minimum in the $C_d(C_l)$ polar, and so B in Eq. (9) contains both AR and δ and any variation of C_d with C_l^2 , much as for the e factor in Eq. (6).

To add to the confusion, the first term of either Eq. (6) or Eq. (8) or Eq. (9) may be referred to as the profile drag or the parasite drag of either the wing system or of the whole airplane. The C_L^2 term is also commonly called *drag due to lift*, which is only partly true in Eq. (8), in which, in fact, the first term has the basic variation of C_d with C_l for the equivalent 2-D wing. It is also identified as the induced drag, which is true for Eq. (8), but only partly for Eqs. (6) and (9), in which it includes all viscous drag that varies with C_l .

B. Actuator Disc Theory

The actuator disc model is used as a quick calculation method for helicopter and propeller analysis [7] and one can find expressions for the induced-power requirement of an actuator disc model of disk area S_d :

$$P_i = \frac{kW^2}{2\rho S_d U} \quad (10)$$

where the factor k accounts for tip losses and nonuniformities over the ideal actuator disc. This formulation is also used [8] in applying the actuator disc model to the flight of birds. Because $P_i = UD_i$ and $S_d = \pi b^2/4$,

$$D_i = \frac{kW^2}{q\pi b^2} \quad (11)$$

and in coefficient form,

$$C_{D,i} = \frac{kW^2}{q^2 S \pi b^2} \quad (12)$$

We may write $b^2 = (bc)b/c = SAR$, and so, in steady, level flight, when $L = W$,

$$C_{D,i} = \frac{kL^2}{q^2 S^2 \pi AR} = \frac{kC_L^2}{\pi AR} \quad (13)$$

Equation (13) agrees with Eq. (3) for the lifting-line model of the fixed wing, if $k = 1/e$ as it is used there. This is the usual inter-

pretation of k as introduced in Eq. (10). The effect of a fixed wing of span b is exactly the same as that of an ideal actuator disc of diameter b . Both devices affect a circle of air with diameter equal to the wing span, or twice the propeller radius, regardless of whether the wing elements move or not. Note carefully, however, that the common nomenclature k in Eq. (13) is not the same as k in Eqs. (4) and (5), in which it is a fitting constant for the variation of viscous drag with C_L^2 such as drawn in Fig. 1. Formulations such as Eq. (13) must be accompanied by another source for taking into account the variation of viscous drag with α or C_l , such as is done in Eq. (8).

C. Practical Calculations

Most engineering and academic institutions will have their own successful way of combining the various drag terms ([9] for example, distinguished between “inviscid” and “viscous” Oswald or span efficiencies) without obvious error, but it is clear that there is potential for confusion and one should not assume that the particular definitions in use are either obvious or are, in fact, correctly described.

Typically, k as used in Eq. (13) is a number slightly above 1, just as e is a number slightly below 1. Glauert [3], in originally tabulating values of δ for various taper ratios of wings with $AR = 2\pi$, had $0.049 \leq \delta \leq 0.016$ for taper ratios (tip cord/root chord) between 1 and 0.25, which gives $0.95 \leq e \leq 0.98$, or $1.05 \leq k \leq 1.02$. These numerical values account only for departures from elliptical loading, and practical values of e and k are then adjusted based on empirical data, so that [4] related that e [in the sense of Eq. (7)] for an entire plane is typically 0.6 for a low-wing plane and 0.8 for a high-wing configuration. Reference [1] gave a table of e values for 15 entire planes ranging from 0.73 for the Cessna C-310 to 0.93 for the Gulfstream G-II (both low-wing), and [7] suggests common values of k between 1.15 and 1.25 for estimating helicopter rotor power requirements. These e values include the parabolic variation of $C_d(C_l)$, as in Eq. (7), and it is most likely that the estimates in [7] for k effectively do the same thing.

Because the final e and k used for aircraft performance analysis are mostly influenced by viscous departures from ideal conditions, their correct calculation will be of increasing importance as the vehicle size and flight speed (hence Reynolds number) decrease. Such performance calculations have yet to become commonplace in micro air vehicle applications, but k or equivalent correction factors are used in the animal-flight literature, when the actuator disc models are often inspired by the actuator disc modeling in helicopter aerodynamics. Thus, k values are often asserted to take similar values: [8] used values of 1.1 for gliding flight calculations and $k = 1.2$ for flapping flight, without further explanation. If $k = 1.2$, then $1/k = e = 0.83$, which is close to the preceding values given for whole planes, but the bird-flight models contain independent expressions for, or assumptions about, profile drag and its variation with α . References [10,11] used a combined modified (pulsed) actuator disc and vortex theory to give temporal and spatial corrections for which the combined effect leads to $k \approx 1.15$. These corrections are therefore in the spirit of the original Eq. (13) and also do not include the $C_d(C_l)$ variation. The downwash distribution close to the trailing edge of the hind wing of a flapping locust at middownstroke has been measured [12] and the departure from the constant value that would be produced by an elliptic loading was used to estimate a value for k , duly reported to be 1.12. Because this value of k attempts to measure only the difference from the ideal elliptic loading, it too falls into the category of $k = 1/e$, where $e = 1/(1 + \delta)$. The general values of k arrived at via various methods in animal-flight studies appear to have values that mimic those in the aeronautics literature, which include the parabolic $C_l(C_d)$ correction, but their derivation and formulation do not include this. It is therefore difficult to evaluate their likelihood of correctness.

The original lifting-line theory gives a perfectly precise definition of e [Eq. (3)], but it is clear that what actually gets used in practical aeronautics is a distant relation only and that between formulation and numerical value there is much empiricism that is rarely clearly detailed.

D. Objectives

Small variations in dimensionless numbers e and k close to 1 may be of minor importance, but their estimation and definition at low Reynolds numbers, when they can have much larger variation, is of much greater import. Furthermore, formulations of e that incorporate the presumed parabolic relationship between C_D and C_L really only hold at moderately high $Re > 5 \times 10^6$ [1]. Here, we make some estimates of e and k for real wings and airfoil sections at moderate Reynolds numbers. The section profile is the Eppler 387, which is famously sensitive to small changes in geometry and angle of attack, with abrupt jumps in $C_l(C_d)$ polars when used below its design Reynolds number [13]. Although it is possible to find airfoils that do not behave this way, many do, and it is also not the abrupt jumps themselves that are of major importance here, but rather the steady reduction in L/D that occurs with declining Reynolds number and that is common to all shapes. Then the validity of the preceding formulations given will be reexamined.

III. Experiments

The lift and drag of an Eppler 387 wing with an aspect ratio of 6 were measured in a low-turbulence wind tunnel, where $u'/U \approx 0.025\%$ for $U = 10$ m/s from hot-wire surveys of the test section with the wing and support removed. The wing span (21 cm) was small compared with the octagonal test section width (1.37 m) and no special tunnel corrections were applied to the data. The wing was milled on a computer-controlled mill with 0.0125 mm resolution, then sanded and painted flat black. The planform was rectangular, with no rounding of the edges at the tip. Two-dimensional experiments were conducted by enclosing the same wing between two end plates suspended by thin cables and with less than 0.3 mm between the wing and the plate. The end plates were aligned carefully with the mean flow and checked for alignment by observing particle traces when the flow was seeded for particle image velocimetry (PIV) experiments. We denote the end-plate condition as 2-D (the basic mean flow configuration is two-dimensional) and the finite aspect ratio case as AR6.

Lift and drag forces were measured with a custom cruciform-shaped force balance that was loaded with four strain gauges on each of the four arms. The measurements were averages of a long time signal (up to 8 s), and the random additive electrical noise in the system allows the effective number of bits in an average measurement to be increased (the 12-bit analog-to-digital converters have an effective number of bits = 18.5 through oversampling of the noisy data) so that forces of 0.05 mN could be resolved. The balance was damped with a parallel dashpot arrangement so that high-frequency mechanical vibrations were not significant, and static calibrations were performed from 0 to 40 mN in 4 mN steps, with a precision of 0.01 mN. At the lowest $Re = 10^4$, one may anticipate drag forces from 0.8 to 5 mN for $0 \text{ deg} \leq \alpha \leq 20 \text{ deg}$, and so the direct calibration data are sparse. Because there was no evidence of nonlinearity over the calibration curve, a linear interpolation back to the origin was used to determine the smallest forces.

The geometric angle of attack α was varied between -10 to 20 deg in steps of 1 deg. Tests were performed for increasing and decreasing α . Repeatability checks were conducted over different days, with new calibrations between days. In the subset of data shown here, the uncertainty of each measurement, as measured by the standard deviation of repeated tests, is approximately given by the symbol size in the graphics. The Reynolds number was varied by changing the tunnel flow speed U . Separate tests, not discussed here, checked the same Reynolds number from different combinations of wing chord c and flow speed U . Reynolds numbers shown here are $Re = 10 \times 10^3$, 20×10^3 , 30×10^3 , and 60×10^3 .

More detailed and extensive results from PIV experiments will be discussed elsewhere, but selected velocity and spanwise vorticity fields will be shown, taken from vertical slices aligned parallel with the mean flow and intersecting the wing at midspan. The velocity fields were estimated using algorithms [14,15] that have been shown to give accurate reconstructions of gradient quantities, and the spanwise vorticity is used to show the flow structure. In these

experiments, the physical configuration is simple, and trials were repeated until both particle seeding properties (density, size, and brightness of particle images) and PIV exposure time (between successive frames) were close to optimal. Then the uncertainty of velocity gradient estimates is likely within 5% of the local maximum.

IV. Results

A. Approximating Lift-Drag Polars at Low Reynolds Numbers

The lift–drag polars of the E387 (in common with many other smooth airfoils) are quite well known for the appearance of unusual features when $Re < 10^5$ [13,16]. These features are usually documented as Reynolds number falls from higher values, but it is also instructive to view the polars with Reynolds number increasing from below. Figure 2 shows the lift–drag polars for Reynolds number increasing from 10×10^3 to 60×10^3 for 2-D and AR6 cases. In the figure, the range of angle of attack α varies slightly from series to series, but is nominally from -10 to 20 deg in increments of 1 deg. Each angle has two data points for increasing and decreasing α . Each Reynolds number is represented by only one series of data points, but the symbol size has been chosen to represent one-half of the maximum standard deviation of repeated independent experiments over one week. For $Re = 10 \times 10^3$ and 20×10^3 , $C_l(C_d)$ curves in Fig. 2a have a c shape, but $C_{l,max}$ is less than 0.8, about half of a typical value of $C_{l,max}$ for moderately thick airfoils at $Re \geq 5 \times 10^5$ (see [4,5,13,17] for numerous examples). For $Re = 30 \times 10^3$, C_l jumps abruptly at $\alpha \approx 10$ deg, rising from about 0.7 to 1.2, with no accompanying change in C_d . C_l then remains

approximately constant, whereas C_d increases from 0.1 to 0.15. The elevated C_l is gradually lost again for $\alpha > 14$ deg, and by $\alpha = 18$ deg the data have returned to the lower Reynolds number curves. In the jump itself, there is hysteresis, as the curves for increasing and decreasing α differ slightly, but repeatably. For $Re = 60 \times 10^3$, the increase in C_l occurs at lower $\alpha = 6.5$ deg and lasts for a longer range of α , up to $\alpha = 19.5$ deg.

As Reynolds number increases, the $C_l(C_d)$ polars shift left: the same C_l is achieved with lower C_d , and the increase in C_d with C_l for $C_l > 0$ is slower. By $Re = 60 \times 10^3$, the initial abrupt increase in C_d , which occurs before the increase in C_l , is seen over a smaller range of α than for $Re = 30 \times 10^3$. With further increases in Reynolds number, the c-shaped curves are recovered, occupying the upper envelope seen in Fig. 2a.

The curves for AR6 wings in Fig. 2b are qualitatively similar to the 2-D case, with two principal differences; the hysteresis has gone from the $Re = 30 \times 10^3$ case, and the decrease in C_D for small $C_L > 0$ with increasing Reynolds number is much more noticeable. At moderate $C_L = 0.4$, $C_D = 0.019$ for $Re = 60 \times 10^3$ and 0.075 for $Re = 10 \times 10^3$. The difference is almost a factor of 4.

The form of curves in Fig. 2 will clearly pose some problems if they are to be modeled as quadratic functions as prescribed, for example, in Eq. (4) and after, or in Eq. (9). Even if such a functional form is appropriate, the shape varies with Reynolds number, and no simple function will successfully capture the sudden increases in C_l or C_L seen in both 2-D and AR6 data.

The success (or lack thereof) of insisting upon a quadratic functional fit to the polar data can be seen by seeking a least-squares fit of C_d on C_l , with the form

$$C_d = a_0 + a_2 C_l^2 \quad (14)$$

where the associations $a_0 = C_{d,0}$ and $a_2 = k$ can be seen in Eq. (5). Figure 3 shows fits of the quadratic function Eq. (14) with $C_d(C_l)$ and $C_D(C_L)$ for 2-D and AR6 wings in the left and right columns, respectively. Because the original data curves are not often simple functions, a second fit is performed in which a particular subset of data points (shown in open symbols) are omitted. These points are associated with the sudden reattachment of the boundary layer and formation of a separation bubble. They are identified by hand and the resulting fit is the dashed line in Fig. 3. The curve fits are least-squares solutions, but no attempt has been made to improve the rather indifferent performance at high Reynolds numbers. The left column of Fig. 3 shows that this fit is not greatly successful at any Reynolds number, with significant differences between the data and the fit curves for almost all practical values of α , where $C_l > 0$. The right column shows that the same result holds for the AR6 wing.

Attempting to fit the entire polar, or even an edited version of it, is difficult. Therefore, one can instead plot $C_d(C_l^2)$ (or $C_D(C_L^2)$) and look for parts close to $C_l = 0$ that can be approximated with a linear fit. Figure 4 shows the result, in which linear least-squares fits are made for the filled symbols at small α . The fit appears moderately successful at $Re = 10 \times 10^3$ and 20×10^3 , but less so at higher Reynolds numbers, when the slope is quite sensitive to subjective choices of data range and uncertainties in the data.

B. Values of e and k at Low Reynolds Number

Even though the curve-fitting exercise is not satisfactory at the higher Reynolds numbers, it is worth calculating the fitting constants as best one can at lower Reynolds numbers to have at least an estimate of the various span efficiency factors. Equations (4–7) may be used as an example of how the drag is estimated from an equation that models the drag through a quadratic variation of C_d with C_l [Eq. (4)] with fitting constant k , and then assumes that k can take the same value for $C_L(C_D)$. Table 1 shows the values of the fitting constants for Eq. (14) as shown by the dashed lines in Fig. 3. The correct procedure is to take the fitting constant $k = a_2$ from the 2-D case (which has no aspect-ratio effect included) and then to insert that k value into an equation that has a separate correction for AR, as in Eqs. (5–7). The fit coefficients are only reasonable for $Re = 10 \times 10^3$ and 20×10^3 when $k = 0.24$ from Table 1.

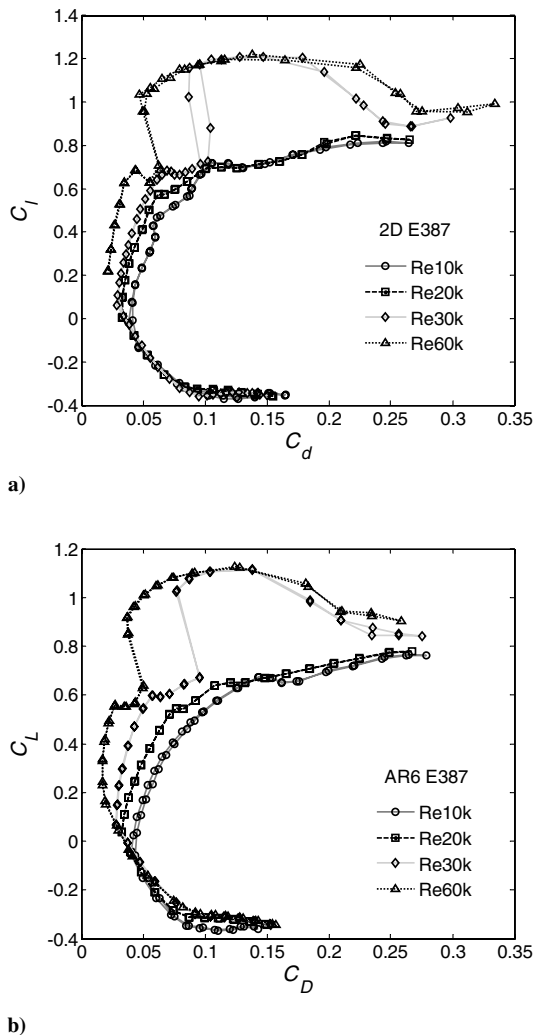


Fig. 2 Lift–drag polars for a) 2-D E387 airfoil section and b) aspect ratio 6 wings.

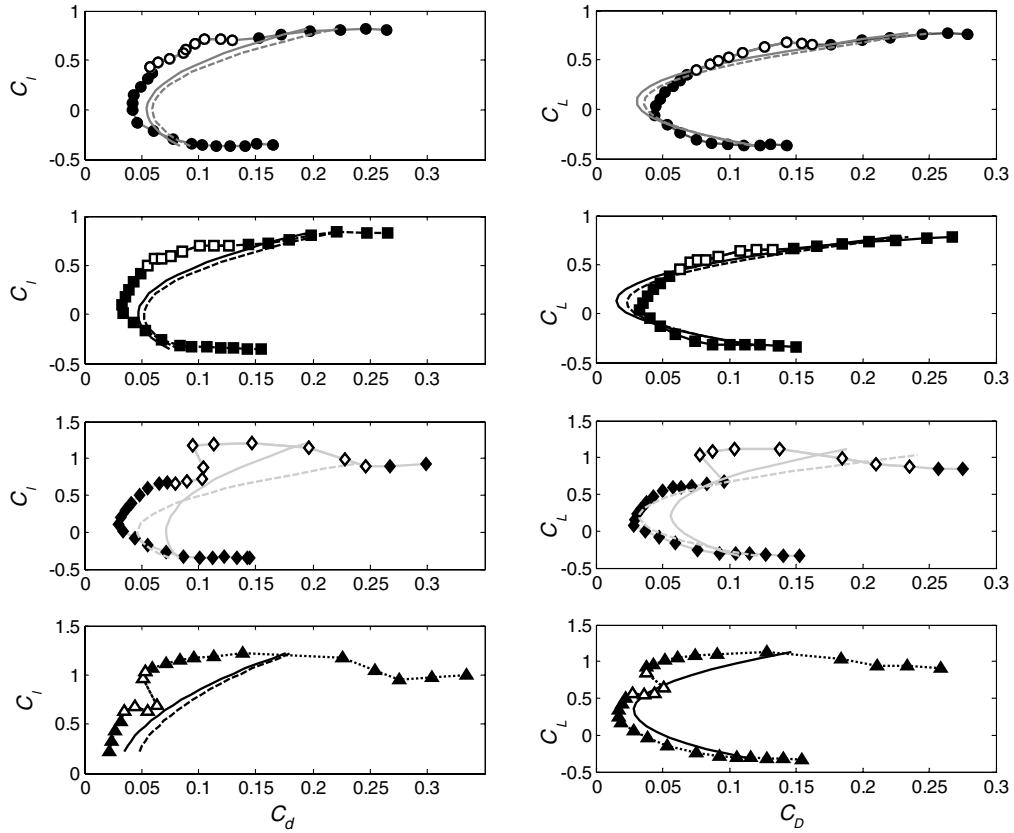


Fig. 3 Lift-drag polars for 2-D (left column) and AR6 (right column) E387 for $Re = 10 \times 10^3, 20 \times 10^3, 30 \times 10^3,$ and 60×10^3 from top to bottom.

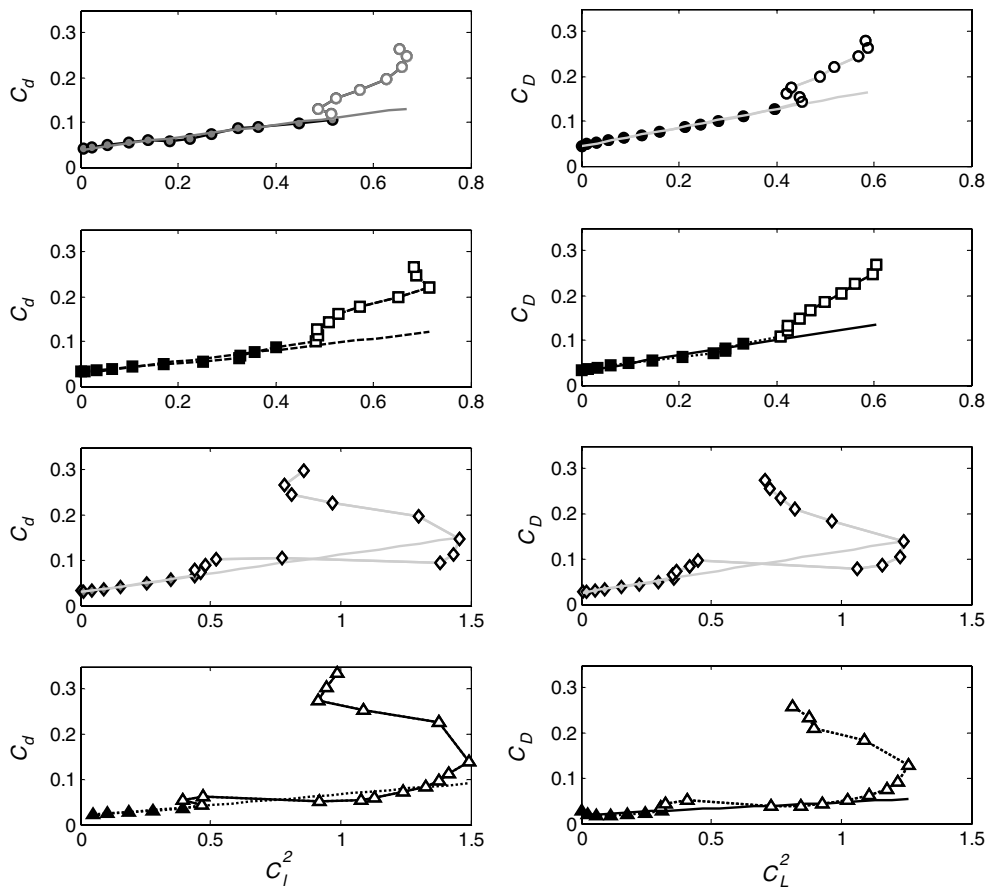


Fig. 4 Plots of $C_d(C_l^2)$ for 2-D airfoil (left) and $C_D(C_L^2)$ for AR6 wing (right) for $Re = 10 \times 10^3, 20 \times 10^3, 30 \times 10^3,$ and 60×10^3 from top to bottom.

Table 1 Coefficients for least-squares quadratic fits of C_d on C_l for 2-D E387 and for C_D on C_L for the AR6 wing

$Re (\times 10^3)$	2-D		AR6	
	a_0	a_2	a_0	a_2
10	0.06	0.24	0.05	0.34
20	0.05	0.24	0.05	0.30
30	0.05	0.22	0.06	0.14
60	0.04	0.09	0.07	0.05

Using Eq. (7) to calculate e , the Oswald efficiency factor, note that $\delta \ll 1$ and $\delta \ll k\pi AR$, and so δ may be neglected, and thus for $AR = 6$,

$$e = \frac{1}{1 + (6 \times 0.24)\pi} = 0.22$$

This value of e is very much lower than any commonly quoted in aeronautics texts, and their example values therefore cannot be applied to low, or moderate, Reynolds number aerodynamics problems.

A similar calculation may be made for the value of e in the sense of Eqs. (3) and (8), when it measures only the departure of the wing loading distribution from the elliptical ideal. Equation (5) can be written as

$$C_D = C_{D,0} + \left(k + \frac{1}{\pi AR e}\right) C_L^2 \quad (15)$$

and the k in brackets is equal to a_2 in Eq. (14). An equivalent quadratic fit for the 3-D AR6 wing gives the whole expression in brackets, and so

$$a_{2,3D} - a_{2,2D} = 1/\pi AR e \quad (16)$$

Taking $a_{2,3D} = 0.34$ and $a_{2,2D} = 0.24$ from Table 1, both for $Re = 20 \times 10^3$, then $e = 10/(\pi AR) = 0.53$. This is much lower than the inviscid result in which $\delta = 0.046$ and $e = 0.96$ for a rectangular nonswept wing of $AR = 6$. It is also lower than commonly reported for higher Reynolds number aeronautical applications. Its inverse, the induced-power factor in actuator disc models, is 1.9, which is considerably higher than commonly assumed values of about 1.2.

One may object that such fits are unduly influenced by rather poor fits through data at higher α , when they are not well approximated by a simple quadratic. Then the procedure can be repeated for the linear fits to $C_d(C_l^2)$ for low α shown in Fig. 4. Table 2 shows these results. Again using the $Re = 10 \times 10^3$ example, the value of e from Eq. (7) uses the fitting constant $k = 0.14$ from Table 2, which gives $e = 0.27$. The difference between coefficients in AR6 and 2-D cases is 0.07, and then the value of e in the sense of Eqs. (3), (8), and (16) is 0.76. These values of e are closer to one than the previous estimates, but are still very low compared with the usual higher Reynolds number examples.

Inspection of Table 2 shows that subtracting 2-D from 3-D fitting coefficients is difficult to do at low Reynolds numbers (one subtracts two numbers for which the difference is comparable with the experimental uncertainty) and completely impractical at higher Reynolds numbers, when the result can be negative. An alternative method for selecting the inviscid part of the e calculation is to take the entire $C_d(\alpha)$ curve and shift it by $C_{D,i} = C_L^2/(\pi AR e)$, as in Eq. (8). Figure 5 shows the result for a range of plausible values of e from 0.5 to 1. The fit depends only weakly on e over this range. The reasonable agreement between the measured AR6 data and the 2-D data incremented by $C_{D,i}$ suggests that the major difficulty in deducing the inviscid part of e is in estimating it from approximate curve fits with low k in the original $C_l(C_d)$ polars.

Table 2 Coefficients for linear fit of $C_d(C_l^2)$ (2-D) and $C_D(C_L^2)$ (AR6) for small α in Fig. 4

$Re (\times 10^3)$	2-D	AR6
10	0.14	0.21
20	0.13	0.17
30	0.08	0.09
60	0.05	0.03

C. Effects of Viscosity

The Oswald efficiency factor of wings at low Reynolds numbers is low because the drag increases faster as a function of lift than at higher Reynolds numbers. It does so because viscosity is more dominant. Friction and pressure drags must always be estimated empirically, even at high Reynolds numbers, and so if the abrupt changes in $C_l(C_d)$ are ignored for the moment, comparatively little changes: the correction coefficients simply have higher or lower values. Although there is no simple analytical theory for the viscous drag coefficients of an arbitrary airfoil section, there are well-established analytical results for the lift, which is basically inviscid. It is therefore of some interest to see whether the lift result alone varies with Reynolds number.

For thin airfoils, the sectional lift coefficient is a linear function of angle of attack, with slope

$$\frac{dC_l}{d\alpha} = C_{l\alpha} = 2\pi \quad (17)$$

From lifting-line theory, an untwisted wing with elliptic loading distribution has a lift coefficient slope that varies systematically with aspect ratio:

$$C_{L\alpha} = 2\pi \left(\frac{AR}{AR + 2} \right) \quad (18)$$

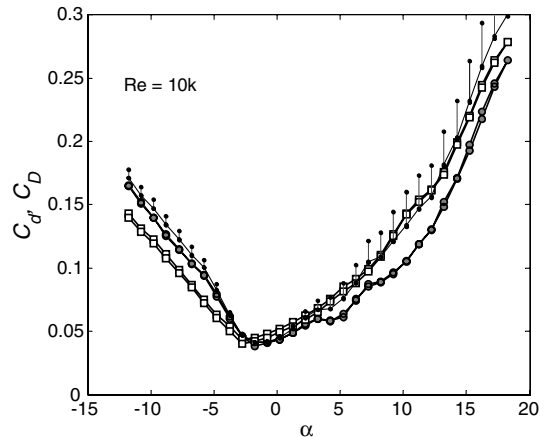
$C_{L\alpha}$ becomes a smaller fraction of $C_{l\alpha}$ as AR decreases. This expression is well-corroborated by experiment until $AR < 4$, when the Helmbold equation,

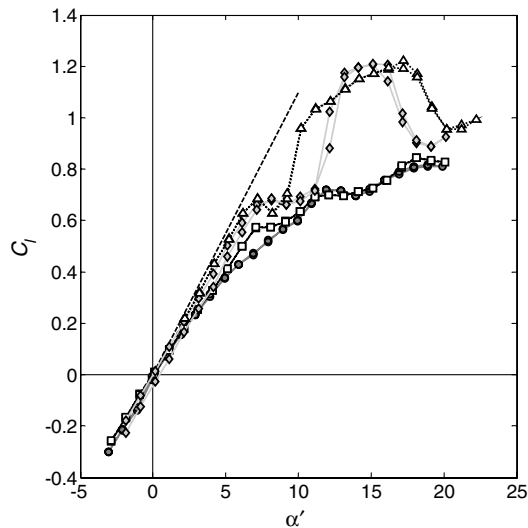
$$C_{L\alpha} = 2\pi \left(\frac{AR}{2 + \sqrt{4 + AR^2}} \right) \quad (19)$$

is a closer fit, as explained in [4,5]. Figure 6 shows $C_l(\alpha')$ for the 2-D case and $C_L(\alpha')$ for the AR6 wing, where α' is the difference in angle of attack from the zero lift angle, and so

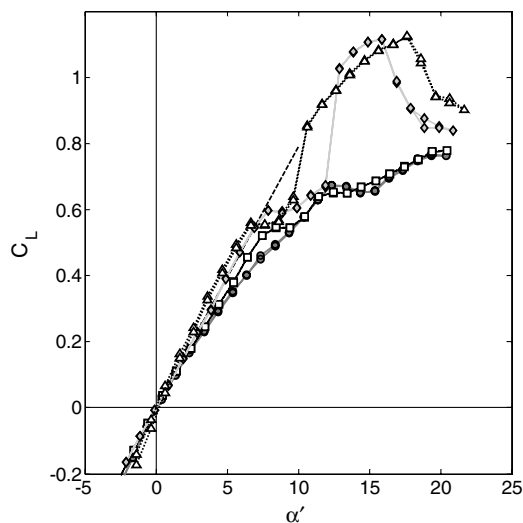
$$\alpha' = \alpha - \alpha_{L=0}$$

At $Re = 60 \times 10^3$, $C_{l\alpha}$ is close to 2π , but it clearly decreases with decreasing Reynolds number. In Fig. 6b, the AR6 case is similar,


Fig. 5 Plots of 2-D measured C_d (circles), 3-D AR6 measured C_D (squares) and predicted 3-D C_D for range of e (small circles joined by straight line).



a)



b)

Fig. 6 Plots of a) $C_l(\alpha')$ for 2-D E387 and b) $C_L(\alpha')$ for AR6 wing with the same section. $Re = 10 \times 10^3$, 20×10^3 , 30×10^3 , and 60×10^3 for circle, square, diamond, and triangle.

where $C_{L\alpha}$ decreases systematically as Reynolds number decreases. At $Re = 60 \times 10^3$, the result is close to that given in Eq. (19), which is shown by the dashed line.

Figure 7 shows the variation of lift coefficient slope with Reynolds number, plotted as a fraction of 2π , which is the 2-D inviscid,

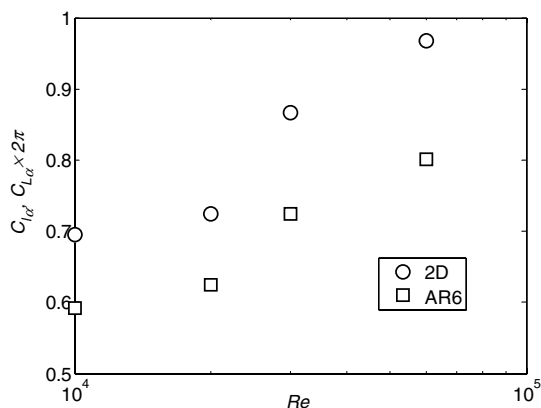


Fig. 7 Slopes $dC_l/d\alpha$ and $dC_L/d\alpha$ from the previous figure, for 2-D and AR6 data, respectively, and $0 \leq \alpha \leq 5$ deg.

analytical result [Eq. (17)]. The dependence on Reynolds number is similar for 2-D and AR6 wings, and power-law fits of $C_{l\alpha} \sim 2\pi Re^\beta$ to the data (there are only four data points) have exponents $\beta = 0.19$ and 0.18 for the 2-D and AR6 wing, respectively. The Reynolds number dependence shows that viscous effects are measurable, even at small α . This is because flow separation begins at the trailing edge of the airfoil/wing, even at small α . Figure 8 shows a time series of spanwise vorticity distributions over and behind the 2-D E387 at $\alpha = 7$ deg, which is when $L/D = (L/D)_{\max} = 5.4$. The time between successive images is 0.1 s, and the shedding frequency is approximately 300 Hz, and so successive images are uncorrelated in time. It is clear that the conditions at the trailing edge are unsteady. Vortex shedding begins at x/c locations that vary with time, but on average are forward of the trailing edge. The mean separation location moves forward as α increases, and at $Re = 10 \times 10^3$ and 20×10^3 , the flow does not reattach. The abrupt performance jumps, where C_l increases and C_d can decrease, occur at higher Reynolds numbers [30×10^3 and 60×10^3 (see Figs. 2a and 2b)] when the separated flow does reattach. Note that reattachment and the presence of a separation bubble are associated with a large increase in C_l/C_d .

V. Discussion

For the E387 wing in the range of $Re \approx 10\text{--}20 \times 10^3$, $e = 0.27$ or 0.76 , depending on whether it is defined to include variations in AR and $C_l(C_d)$ [Eq. (7)] or whether it is only the inviscid-model departure from an ideal, elliptically loaded, wing [Eq. (3)]. The associated values of the induced-power correction factor in actuator disc theory are 3.7 and 1.3, respectively. These values are much further from 1 than in any example in the aeronautics literature or used in the animal-flight literature. This is because no example has hitherto been based on data at low Reynolds numbers. In fact, the shapes of the $C_l(C_d)$ and $C_L(C_D)$ polars for 2-D airfoils and fixed-wings are not well approximated by the parabolic shape demanded by theory at these Reynolds numbers, and for the two higher Reynolds numbers included in this study, $Re = 30 \times 10^3$ and 60×10^3 , it is hardly worth trying to fit the curves with simple parabolas.

The mutually contradictory definitions of the span efficiency e that appear in the technical literature make it difficult to trace the context of reported values of k and e , which are often given without detailed reasoning or supporting evidence, partly because, even in simple aircraft, there are many empirical contributions and approximations contained in the final sum. For clarity, it is proposed that the two common definitions be distinguished through subscripts, so that

$$e_i = 1/(1 + \delta) \quad (20)$$

is the inviscid span efficiency. It is determined only by the small parameter δ that comes exclusively from departures of the wing loading distribution from elliptical. Then $k_i = 1/e_i$ is an induced-power factor that can be used in the sense of Eq. (13). Likely inviscid departures of e_i and k_i from 1 are comparatively small, as they do not include effects of finite span or practical lift-drag-polar shapes. The second definition of span efficiency might be as used in Eq. (7), repeated here for convenience:

$$e_v = 1/(1 + \delta + k\pi AR) \quad (21)$$

By inspection, e_v contains both the effect of aspect ratio and the approximate shape of the lift-drag polar in the form of fitting constant k . This may be termed a wing efficiency factor and its inverse is $k_v = 1/e_v$. Values of e_v may be much less than 1.

It is really only useful to use the second form of efficiency factor e_v if the section lift-drag polar can be approximated by a simple quadratic equation, as written in Eqs. (4) and (5). If such a fit is not adequate, as is the case for the airfoils and wings reported here, then it is better to use e_i as the measure of inviscid distribution efficiency and to retain some more complete empirical $C_l(C_d)$ relation. This would be a lookup table of polars such as Fig. 2a, and then the appropriate expression for a total drag coefficient would be of the form of Eq. (8), in which the viscous and inviscid parts are kept separate. This

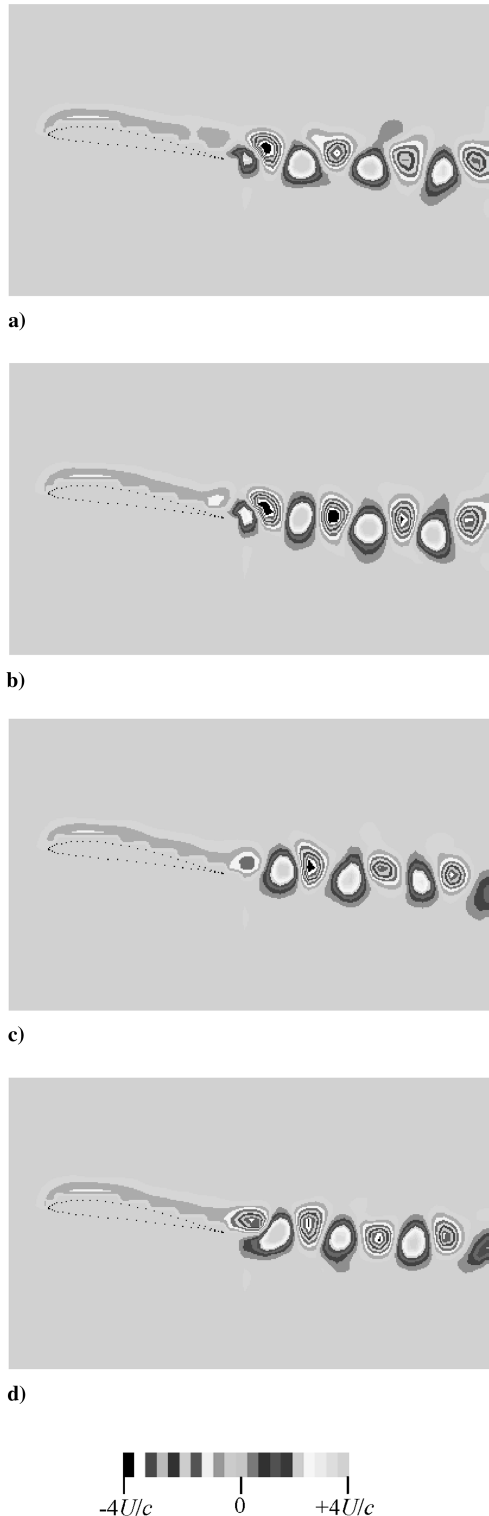


Fig. 8 Four snapshots of the spanwise vorticity field over the E387 at $\alpha = 7$ deg. $Re = 11.7 \times 10^3$. The image window size $\Delta x, \Delta z = 2.7$ and $1.3c$. The mean flow is from left to right. The shape of the contours immediately next to the wing outline is stepped due to the limited spatial resolution there.

requires an accurate knowledge of $C_l(C_d)$ for the wing sections at the correct Reynolds number, and such reliable data are not yet common for $Re < 10^5$.

The failure of standard aeronautical methods to account for the low Reynolds number performance is due to the sensitivity of the airfoil or wing performance to separation location [18]. Although only the particular case of the E387 has been examined here, the

lift–drag polar is not atypical of smooth airfoil sections at such low Reynolds numbers. For example, a collection of data specifically targeted at the aeromodeling community at low Reynolds numbers [19] shows qualitatively similar profiles for the Clark-Y, N60R, Go 790 series, NACA 4412, E374 and E205, among others. Moreover, as noted in the Introduction, it is not the possibly large variations in $C_l(C_d)$ that cause the very large values of k (or small values of e), which are derived from smooth curve fits that ignore such features. The small e and large k come from the systematic boundary-layer separation forward of the trailing edge, which causes not only the relatively large drag coefficients, but also the systematic departures in lift coefficient from the inviscid prediction.

The results here show that estimations of induced or total drag coefficients that involve nominally small corrections may not work very well when $Re < 10^5$. By contrast, the lift of various flat-plate planforms has been found [20] to depart very little from inviscid theory for $8 \times 10^3 \leq Re \leq 24 \times 10^3$. However, the wings in question had a very low $AR = 2$, and the finite span and associated velocity field induced at the tip will have dominated the performance measurement. Here, the Reynolds number dependence is clear for $AR = 6$, which is not very different from classes of small-scale flying devices that would include practical micro air vehicles, birds, and bats.

In any extrapolation of these results to animal flight in particular, we should note that even in gliding flight, animal wings show considerable variation in section profile geometry and local twist along the span. The wings also flex according to the aerodynamic loads and may be partly porous, and the planform can be varied with flight speed and ambient conditions. It is not yet known which of these many complications and subtleties are important, but it is quite unlikely that a one-parameter model fit will do the physics justice. Furthermore, because the rather high effective values of k will send the bird-flight model predictions far from observational data, one might argue that the existing reasonable fit with much lower, more standard, values of k implies that the real bird wing has a much better control of the boundary-layer separation than does a fixed-wing model at these Reynolds numbers. This argument applies equally to bird and bat wings in both gliding and flapping flight.

VI. Conclusions

When corrections to a basic model are on the order of 10% or less, they do not necessarily subvert the model basis itself, and uncertainties in the values of the corrections themselves may not be of great concern. Here, we see that for fixed-wings operating at $Re < 10^5$, not only can the corrections be large in magnitude, but there is uncertainty in the formulation of the corrections themselves. This is perhaps a sign that new theoretical models are required for airfoils in which viscosity cannot be neglected, even at low angles of attack. Such theories could at first be empirically based, if the supporting high-quality data were available. In the long term, more fundamental improvements in formulations that predict both lift and drag would be highly desirable. These advances would have immediate impact in application to the flight performance of various small-scale flying devices.

References

- [1] Lan, C.-T. E., and Roskam, J., *Airplane Aerodynamics and Performance*, DARCorporation, Lawrence, KS, 1997.
- [2] Prandtl, L., “Applications of Modern Hydrodynamics to Aeronautics,” NACA TR 116, 1921.
- [3] Glauert, H., *The Elements of Aerofoil and Airscrew Theory*, Cambridge Univ. Press, Cambridge, England, U.K., 1948.
- [4] McCormick, B. W., *Aerodynamics, Aeronautics and Flight Mechanics*, Wiley, New York, 1995.
- [5] Anderson, J. D., *Fundamentals of Aerodynamics*, McGraw–Hill, New York, 2007.
- [6] von Mises, R., *Theory of Flight*, McGraw–Hill, New York, 1945.
- [7] Leishman, J. G., *Principles of Helicopter Aerodynamics*, Cambridge Univ. Press, Cambridge, England, U.K., 2006.
- [8] Pennycuik, C. J., *Modelling the Flying Bird*, Academic Press, London, 2008.

- [9] Traub, L. W., "Analytic Drag Prediction for Cambered Wings with Partial Leading-Edge Suction," *Journal of Aircraft*, Vol. 46, No. 1, 2009, pp. 312–319.
doi:10.2514/1.38558
- [10] Ellington, C. P., "The Aerodynamics of Hovering Insect Flight, 5: A Vortex Theory," *Philosophical Transactions of the Royal Society of London, Series B: Biological Sciences*, Vol. 305, No. 1122, 1984, pp. 115–144.
doi:10.1098/rstb.1984.0053
- [11] Ellington, C. P., "The Aerodynamics of Hovering Insect Flight, 6: Lift and Power Requirements," *Philosophical Transactions of the Royal Society of London, Series B: Biological Sciences*, Vol. 305, No. 1122, 1984, pp. 145–181.
doi:10.1098/rstb.1984.0054
- [12] Bomphrey, R. J., Taylor, G. K., Lawson, N. J., and Thomas, A. L. R., "Digital Particle Image Velocimetry Measurements of the Downwash Distribution of a Desert Locust *Schistocerca Gregaria*," *Journal of the Royal Society Interface*, Vol. 3, No. 7, 2006, pp. 311–317.
doi:10.1098/rsif.2005.0090
- [13] Lyon, C. A., Broeren, A. P., Giguere, P., Gopalarathnam, A., and Selig, M. S., *Summary of Low-Speed Airfoil Data*, Vol. 3, Soartech, Virginia Beach, VA, 1997.
- [14] Fincham, A. M., and Spedding, G. R., "Low-Cost, High Resolution DPIV for Measurement of Turbulent Fluid Flow," *Experiments in Fluids*, Vol. 23, No. 6, 1997, pp. 449–462.
doi:10.1007/s003480050135
- [15] Fincham, A. M., and Delerce, G., "Advanced Optimization of Correlation Imaging Velocimetry Algorithms," *Experiments in Fluids*, Vol. 29, No. 7, 2000, pp. S013–S022.
doi:10.1007/s003480070003
- [16] Spedding, G. R., Hedenström, A., McArthur, J., and Rosén, M., "The Implications of Low-Speed Fixed-Wing Aerofoil Measurements on the Analysis and Performance of Flapping Bird Wings," *Journal of Experimental Biology*, Vol. 211, No. 2, 2008, pp. 215–223.
doi:10.1242/jeb.007823
- [17] Abbot, I. H., and von Doenhoff, A. E., *Theory of Wing Sections*, Dover, New York, 1959.
- [18] Lissaman, P. B. S., "Low Reynolds Number Airfoils," *Annual Review of Fluid Mechanics*, Vol. 15, 1983, pp. 223–239.
doi:10.1146/annurev.fl.15.010183.001255
- [19] Simons, M., *Model Aircraft Aerodynamics*, Special Interest Model Books, Ltd., Poole, England, U.K., 1999.
- [20] Kaplan, S. M., Altman, A., and Ol, M., "Wake Vorticity Measurements for Low Aspect Ratio Wings at Low Reynolds Number," *Journal of Aircraft*, Vol. 44, No. 1, 2007, pp. 241–251.
doi:10.2514/1.23096